RESEARCH ARTICLE OPEN ACCESS

Innate Immunity

VSIG4-Expressing Macrophages Contribute to Antiparasitic and Antimetastatic Responses in the Peritoneal Cavity

Els Lebegge[1,2] | Daliya Kancheva[1,2,3] | Jolien Van Craenenbroeck[1,2] | Sam Ernst[4,5,6] | Pauline M. R. Bardet[1,3] | Aarushi A. Caro[1,3] | Máté Kiss[1,2] | Neema Ahishakiye Jumapili[1,2] | Romina Mora Barthelmess[1,2] | Maida Zivalj[1,2] | Naela Assaf[1,2] | Leen Ali[2,7] | Yvon Elkrim[1,2] | Jesse Demuytere[4,5,6] | Jan De Jonge[8] | Geert Raes[1,2,3] | Eva Hadadi[1,2,3] | Nick Devoogdt[8] | Cécile Vincke[1,2] | Kiavash Mohavedi[7] | Lars Vereecke[9,10,11] | Wim Ceelen[4,5,6] | Benoit Stijlemans[1,2] | Damya Laoui[1,3] | Sana M. Arnouk[1,2] | Jo A. Van Ginderachter[1,2]

[1]Laboratory of Cellular and Molecular Immunology, Brussels Center for Immunology (BCIM), Vrije Universiteit Brussel, Brussels, Belgium | [2]Laboratory of Myeloid Cell Immunology, VIB Center for Inflammation Research, Brussels, Belgium | [3]Laboratory of Dendritic Cell Biology and Cancer Immunotherapy, VIB Center for Inflammation Research, Brussels, Belgium | [4]Department of GI Surgery, Ghent University Hospital, Ghent, Belgium | [5]Laboratory of Experimental Surgery, Ghent University, Ghent, Belgium | [6]Cancer Research Institute Ghent (CRIG), Ghent University, Ghent, Belgium | [7]Brain and Systems Immunology Lab, Brussels Center for Immunology (BCIM), Vrije Universiteit Brussel, Brussels, Belgium | [8]Laboratory of Molecular Imaging and Therapy (MITH), Vrije Universiteit Brussel, Brussels, Belgium | [9]Department of Internal Medicine and Pediatrics, Ghent University, Ghent, Belgium | [10]VIB-UGent Center for Inflammation Research, Ghent, Belgium | [11]Ghent Gut Inflammation Group (GGIG), Ghent, Belgium

Correspondence: Jo A. Van Ginderachter (jo.van.ginderachter@vub.be)

ABSTRACT

Large peritoneal macrophages (LPMs) play a role as gatekeepers of peritoneal homeostasis by providing a first line of defense against pathogens. A third of the LPMs express the surface receptor VSIG4, but it is unclear whether these cells differ from their VSIG4-negative counterparts and perform dedicated functions. We demonstrate that VSIG4+, but not VSIG4−, LPMs are in the majority derived from embryonal precursors, and their occurrence is largely independent of sex and microbiota but increases with age. Although their transcriptome and surface proteome are indistinguishable from VSIG4− LPMs at steady-state, VSIG4+ LPMs are superior in phagocytosing *S. aureus* bioparticles and colorectal carcinoma (CRC) cells. Anti-VSIG4 nanobody constructs that are ADCC-enabled allowed a selective elimination of the VSIG4+ LPM subset without affecting overall LPM abundance. This strategy uncovered a role for VSIG4+ LPMs in lowering the first peak of parasitemia in a *Trypanosoma brucei brucei* infection model and in reducing CRC outgrowth in the peritoneal cavity, a prime metastatic site in CRC patients. Altogether, our data uncover a protective role for VSIG4+ LPMs in infectious and oncological diseases in the peritoneal cavity.

1 | Introduction

In the peritoneal cavity (PC) at steady-state, two subsets of tissue-resident macrophages have been described based on their morphology and function, termed "small" and "large" peritoneal macrophages (SPMs and LPMs) [1]. Disturbance of homeostasis in the PC leads to LPM activation, followed by their adhesion and cellular clot formation, disappearance from the PC, and migration to the omentum [2]. Of interest, a subset of LPMs expresses the V-set and Immunoglobulin domain containing 4 receptor (VSIG4), which is a member of the B7-protein family and is also referred to as the complement receptor of the immunoglobulin superfamily (CRIg) [3, 4]. However, it is currently unclear to what extent the VSIG4+ and VSIG4− LPM subsets differ and whether they have dedicated functions.

VSIG4 ligand binding, which leads to receptor internalization, can occur in complement-dependent, for example, C3-opsonized particles, and in a complement-independent manner, for example, lipoteichoic acid binding on Gram-positive bacteria [3, 5]. VSIG4 receptor signaling in macrophages suppresses their pro-inflammatory activation through metabolic changes, leading to reduced mitochondrial reactive oxygen species production [6]. Besides these macrophage-intrinsic effects, the VSIG4 receptor can also suppress T-cell activation and T-cell-mediated responses, either by directly binding to an as yet unidentified receptor on T cells or via complement proteins that bridge the VSIG4 receptor and a complement receptor on T cells [4, 7, 8]. Hence, the VSIG4 receptor is able to modify both innate (macrophage-mediated) and adaptive immunity and is therefore an interesting target for the treatment of macrophage-driven pathologies [9].

For this reason, we explored the potential differences between VSIG4+ and VSIG4− LPMs, the function of the VSIG4 receptor, as well as the possibility of targeting VSIG4+ LPMs. scRNA-seq and CITE-seq data showed a lack of transcriptomic and proteomic differences between VSIG4+ and VSIG4− LPMs at steady-state and during an infection with African trypanosomes, but VSIG4+ LPMs demonstrated an increased phagocytic capacity. A specific depletion of VSIG4+ LPMs via a newly generated anti-VSIG4-antibody-dependent cell-mediated cytotoxicity (ADCC) construct led to an enhanced first peak of *Trypanosoma* parasitemia and a faster peritoneal dissemination of colorectal carcinoma (CRC) cancer cells, showing a protective function of this peritoneal macrophage population in such disease settings.

2 | Results

2.1 | VSIG4 Marks a Subset of Large Peritoneal Macrophages (LPMs) that is Ontogenically Different from VSIG4-Negative LPMs and is Maintained Regardless of Sex and Microbiota

To assess VSIG4 expression on the PC CD45+ hematopoietic compartment, a lavage from the steady-state PC of female C57BL/6 mice was analyzed. LPMs can be identified through their high F4/80 and ICAM2 expression (Figure 1A), with approximately one-third of these cells expressing high levels of the VSIG4 receptor. TIM4 [10, 11] and CD206 [12, 13] expression were previously also used to identify LPM subsets, so we assessed these markers on LPMs with a differential VSIG4 expression. While the vast majority of VSIG4+ LPMs expressed the TIM4 receptor, a small population of VSIG4+ TIM4− LPMs (3.4% of total LPMs) was present in peritoneal lavages of naive female mice (Figure S1A). Conversely, VSIG4 was absent on SPMs and other CD45+ cell types in a naive peritoneal lavage (Figure 1B). Only 1.1% of LPMs expressed the CD206 receptor, mainly VSIG4− LPMs (Figure S1A). Unlike the clear distinction in VSIG4 expression, all LPMs equally expressed CD64, CD74, CD204, CD14, CD274, CD163 and CD169 (Figure S1B).

In age-matched male mice, the overall percentage of LPMs in the PC was not significantly different from females (Figure S2A), but the percentage of VSIG4+ cells within that population was on average 5% lower (Figure S2B). Of note, the VSIG4 surface expression level was not significantly different between male and female VSIG4+ LPMs but tended to be lower in the latter (Figure S2C). Bain et al. [14] demonstrated that the percentage of VSIG4+ LPMs increased with age in female mice. In agreement, we observed a near doubling in the percentage of VSIG4+ LPMs (within total LPMs) in 10-month-old female mice (45 ± 6.93%) as compared with 6-week-old female mice (26.3 ± 1.43%) (Figure S2D).

Like many tissue-resident macrophages, the LPM pool is sustained via the proliferation of embryonic LPMs, but can also be replenished by bone marrow-derived monocytes [15, 16]. To assess the ontogeny of VSIG4+ and VSIG4− LPMs, Flt3-driven YFP-reporter mice were used, in which YFP+ cells are of bone marrow monocytic origin [17]. Interestingly, approximately 60% of VSIG4+ LPMs were YFP-negative and hence of embryonic origin, while the majority (70%) of VSIG4− LPMs were YFP-positive and hence of bone marrow origin (Figure 1C). Thus, although VSIG4 expression is mostly associated with embryonic LPMs, this receptor can also be acquired by monocyte-derived cells.

Since VSIG4 functions as a pattern-recognition receptor, the presence of bacterial molecules could be another factor regulating VSIG4 expression by LPMs. Indeed, previous work demonstrated an impact of the microbiota on peritoneal macrophages [18], prompting us to ask whether the gut microbiome could affect VSIG4+ LPMs. In germ-free (GF) mice, the percentage of LPMs within CD45+ peritoneal cells was significantly lower as compared with age-matched conventional mice (Figure 1D), but within the LPM population, an equal contribution of VSIG4+ cells was observed (Figure 1E). However, the VSIG4 expression level was significantly higher in VSIG4+ LPMs of GF mice (Figure 1F), suggesting that intestinal microbes or their derived factors may restrain VSIG4 surface expression but do not fundamentally affect the generation of VSIG4+ LPMs.

2.2 | Steady-state VSIG4+ and VSIG4− LPMs are Identical at the Transcriptomic and Surface Proteomic Level, but VSIG4+ LPMs are Superior Phagocytes of *S. aureus* Bioparticles

Since VSIG4 signaling is able to affect the macrophage activation state [6], it is conceivable that VSIG4-expressing LPMs may be differently activated from their VSIG4-negative counterparts. To
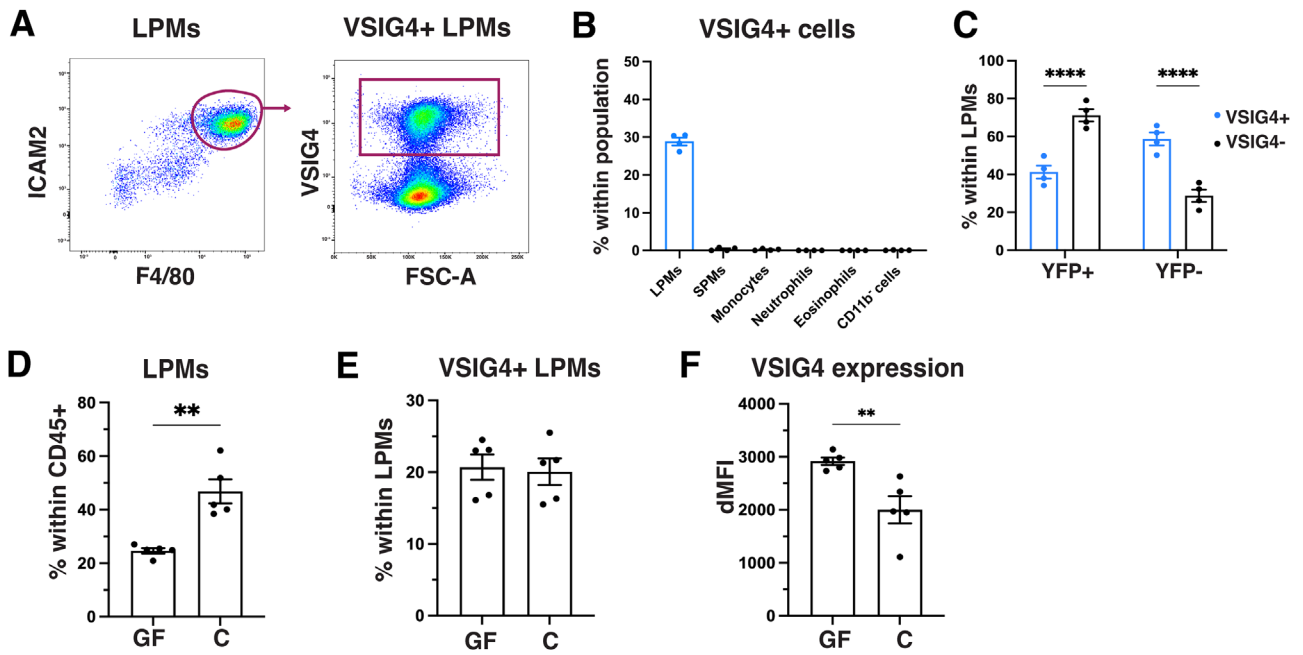
FIGURE 1 | VSIG4 marks a subset of large peritoneal macrophages (LPMs) in the peritoneal cavity. (A) Representative gating strategy for the identification of VSIG4$^+$ LPMs in a naive peritoneal lavage of female C57BL/6 mice. (B) Percentage of VSIG4$^+$ cells within each immune cell population in a naive peritoneal lavage of female C57BL/6 mice ($n = 4$). Data are representative of two independent experiments. (C) Percentage of YFP$^+$ and YFP$^-$ cells within VSIG4$^+$ and VSIG4$^-$ LPMs of naive Flt3-Cre x ROSA26-YFP mice ($n = 4$). (D) Percentage of LPMs within CD45$^+$ cells, (E) percentage of VSIG4$^+$ LPMs within all LPMs, and (F) VSIG4 expression level in VSIG4$^+$ LPMs depicted as ΔMFI in naive germ-free C57BL/6 mice compared with conventional mice ($n = 5$/group). Unpaired two-tailed Student's t-tests were performed. The p-value is shown on the graphs as such: *$p \leq 0.05$, **$p \leq 0.01$, ***$p \leq 0.001$, ****$p \leq 0.0001$. Data are shown as the mean ± SEM.

evaluate differences between steady-state VSIG4$^+$ and VSIG4$^-$ LPMs at the transcriptomic level, LPMs were in the first instance extracted from the publicly available dataset by Bain et al. [12], encompassing peritoneal cells from female and male mice, based on the expression of tissue-resident LPM markers (*C1qa, Cd9, Gata6, Icam2, Timd4, Prg4, Calml4, Prtn3*) and exclusion of clusters with T cell (*Cd3e, Cd3g, Cd2*), monocyte (*Ccr2, Ly6c2, Plac8, Ear2*) and DC (*Flt3, H2-Aa, Itgax, Cd209a, Slamf7, Pldb1*) specific genes. Four LPM clusters were obtained after excluding proliferating cells from the scRNAseq dataset (Figure 2A,B), with all clusters expressing variable levels of prototypical LPM genes such as *Adgre1, Timd4, Icam2, Cd9, C1qc, C1qb* and *Cd68* (Figure 2A). These LPM genes were most prominently expressed by the small cluster 3, which also expresses the highest levels of *Marco* (Figure 2A). Cluster 1 most prominently expressed *Sdc3, Wfdc17, Atp5e* and *Rpl22l1* and cluster 2 was characterized by *Folr2, Ccl6, Retnla, Mrc1, Ccr2* and genes linked to MHC-II expression (*Cd74, H2-Aa, H2-Ab1*) (Figure 2A). Remarkably, *Vsig4* expression was spread across all LPM subsets, all of which were partially *Vsig4$^+$*, with the lowest expression level seen in cluster 2 and the highest in cluster 0 (Figure 2B,C). When the entire LPM population was separated into a *Vsig4$^+$* and a *Vsig4$^-$* subset, no significantly differentially expressed genes (DEGs, with a fold change higher than 1) were discovered, except for the *Vsig4* gene itself (Figure 2D). Of note, when analyzing samples from female and male mice separately, the same LPM subsets were detected in both sexes (Figure S3A,B), no transcriptomic differences were found between female and male *Vsig4$^+$* LPMs (Figure S3C), and only a few genes were differentially expressed between *Vsig4$^-$* LPMs in both sexes (Figure S3D). Moreover, no DEGs (except

Vsig4) were found between *Vsig4$^+$* and *Vsig4$^-$* LPMs, either in females or males (Figure S3E,F).

To assess potential differences between steady-state VSIG4$^+$ and VSIG4$^-$ LPMs at the surface proteome level, cellular indexing of transcriptomes and epitopes (CITE)-sequencing analysis on peritoneal lavages of female C57BL/6 mice was performed (Table S2 for the list of barcoded antibodies), incorporating barcoded anti-VSIG4 antibodies [19]. This newly generated dataset again revealed LPM heterogeneity based on transcriptomic differences (Figure 2E; Figure S4) and, similar to the *Vsig4* mRNA expression pattern, the VSIG4 protein was expressed at the surface across all different LPM subsets (Figure 2F). Consequently, when LPMs were split into VSIG4$^+$ and VSIG4$^-$ subsets, hardly any differentially expressed genes (DEGs) nor proteins (DEPs) were detected between naive VSIG4$^+$ and VSIG4$^-$ LPMs (Figure 2G,H). In conclusion, at steady-state, no transcriptomic nor surface proteomic differences can be observed between VSIG4$^+$ and VSIG4$^-$ LPM subsets, except VSIG4 itself.

Finally, we assessed whether the expression of VSIG4, which can serve as a pattern recognition receptor by binding lipoteichoic acid in the cell wall of Gram-positive bacteria such as *Staphylococcus aureus* [5], confers a superior bacterial uptake capacity to LPMs. To this end, the phagocytic capacity of VSIG4$^+$ and VSIG4$^-$ LPMs toward PhRodo-labeled *S. aureus* and Gram-negative *E. coli* bioparticles (BP) was tested, by injecting these BP in the PC of naïve female C57BL6 mice and collecting peritoneal lavages 10 min later. A significantly increased uptake of *S. aureus* BP, but not *E. coli* BP, was observed by VSIG4$^+$ LPMs compared
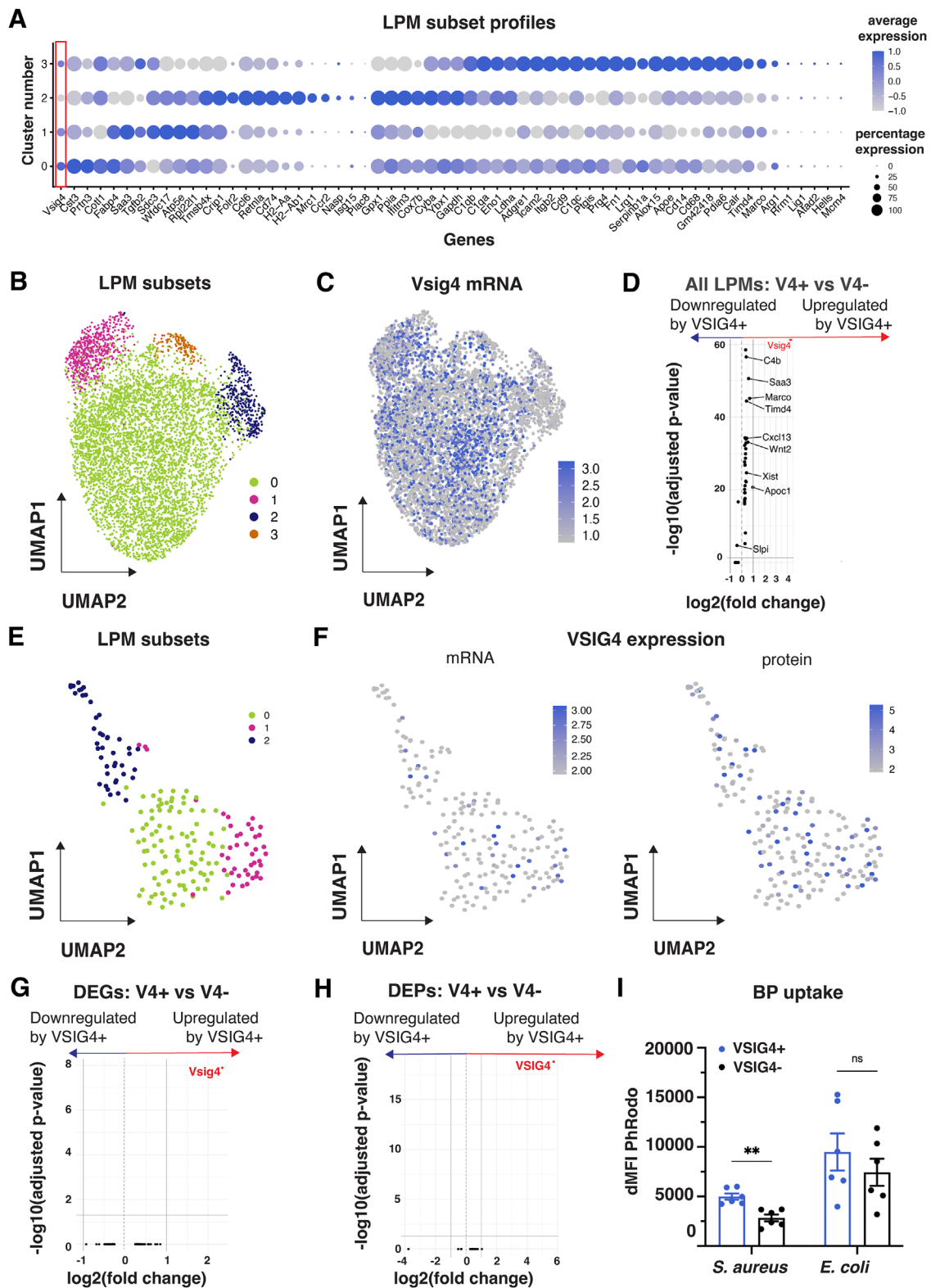
FIGURE 2 | VSIG4+ LPMs are superior phagocytes for Gram-positive bacteria, despite being identical at the transcriptomic and surface proteomic level in steady state. (A) Dot plot of highly expressed markers per LPM cluster obtained from the scRNA-sequencing dataset by Bain et al. [14]. The size of the dot indicates the expression percentage in the LPM subset, while the color indicates the average expression level. (B) UMAP plot of LPM clusters obtained from the scRNA-sequencing dataset by Bain et al. [14]. (C) Feature plot of *Vsig4* mRNA expression in LPM subsets. (D) Volcano plot of differentially expressed genes (DEGs) between *Vsig4*+ and *Vsig4*− LPMs, whereby the adjusted *p*-value is plotted versus the fold change. LPMs were divided into *Vsig4*+ and *Vsig4*− based on the mRNA expression cut-off of >2 and 0, respectively. (E) UMAP plot of LPM clusters obtained via CITE-sequencing of peritoneal exudate cells obtained from control i.p. HBSS-injected mice. Peritoneal lavages of 3 naïve animals were pooled. (F) Feature plot of *Vsig4* mRNA and VSIG4 protein expression in LPM subsets. Volcano plot of DEGs (G) and differentially expressed proteins (DEPs) (H) between VSIG4+ and VSIG4− LPMs, whereby the adjusted *p*-value is plotted versus the fold change. LPMs were divided into VSIG4+ and VSIG4− LPMs based

with VSIG4⁻ LPMs (Figure 2I). Hence, despite being identical at steady-state, VSIG4 expression confers a competitive advantage to VSIG4⁺ LPMs to phagocytose *S. aureus* BP.

2.3 | A Specific Nanobody-Mediated Depletion of VSIG4⁺ LPMs Demonstrates Their Influence on Early Phase *Trypanosoma brucei brucei* Infections Without Effect on Chronic Disease Outcome

VSIG4 is also known to play a role in the phagocytic uptake of African trypanosomes, such as *Trypanosoma brucei brucei* [19]. Therefore, we injected live *T. b. brucei* parasites in the PC and assessed the response of LPMs 18 h later. At that timepoint, the percentage of LPMs within the total CD45⁺ population (Figure 3A), as well as the absolute number of LPMs (Figure S5A), tended to be reduced in infected mice compared with naïve mice, albeit not significantly. Absolute numbers of VSIG4⁺ LPMs (and their percentage within total LPMs, Figure 3B) and CD45⁺ hematopoietic cells were also similar in naïve and infected mice (Figure S5A–C). Interestingly, the VSIG4 surface expression level on VSIG4⁺ LPMs decreased in infected mice (Figure 3C), possibly reflecting receptor internalization upon binding [3].

CITE-sequencing uncovered novel LPM clusters in infected mice compared with the naïve controls (Figure 3D,E). Indeed, while cells belonging to clusters 0, 1, and 2 could be found in both naive and infected mice, cluster 3 (characterized by *Ccl6, Saa3, Sdc3, Ldha*, and *Arg1*) were almost exclusively found in the infected PC (Figure 3E; Figure S5D). Upon reclustering of LPMs from *T. brucei brucei*-infected mice only, *Vsig4* mRNA as well as VSIG4 protein were expressed across all LPM subsets, akin to the naïve situation (Figure 3F). An increased gene expression of *Ccl6* and *Saa3* was detected in VSIG4⁺ LPMs of infected mice compared with naïve VSIG4⁺ LPMs (Figure 3G), suggestive of a somewhat more inflammatory phenotype [20–22]. In accordance, at the protein level, VSIG4⁺ LPMs of infected mice showed an upregulation of proteins related to macrophage activation (MHC-II, CD172a, CD55, Ly6A), migration (CD105, CD102, CD63), as well as modulation of the adaptive immune response (CD80, CD86, CD274, CD150) as compared with naïve VSIG4⁺ LPMs (Figure 3H). However, no significant DEGs nor DEPs, except for *Vsig4/*VSIG4, were detected between VSIG4⁺ and VSIG4⁻ LPMs in the infected PC (Figure 3I,J).

To directly investigate the role of VSIG4⁺ LPMs during a *T. b. brucei* infection, we developed a strategy for the specific elimination of this LPM subset. An anti-VSIG4-ADCC construct was designed by fusing an ADCC-enabled mouse IgG2a Fc tail to two copies of a mouse VSIG4-binding VHH, that was previously generated by our lab [23] (Figure 4A). As a non-depleting control, an ADCC-disabled construct was generated by introducing a LALAPG mutation in the IgG2a Fc-tail [24]. Seven days after a single intraperitoneal injection of the anti-VSIG4-ADCC construct in naïve female animals, the majority

of VSIG4⁺ LPMs were depleted, while this was not the case with the ADCC-disabled construct (Figure 4B). VSIG4⁺ LPMs remained largely absent for at least another 2 weeks. Importantly, the percentage of total LPMs in the PC remained unaltered upon depletion, suggesting a rapid replenishment of the total LPM pool, albeit without VSIG4 expression (Figure 4C). As a matter of fact, VSIG4⁺ LPMs did not fully recover by day 56 post-depletion, illustrating that regaining the VSIG4⁺ phenotype is a slow process (Figure 4B). As an important control, VSIG4⁺ Kupffer cell (KC) numbers were not affected at any time point by the intraperitoneal anti-VSIG4-ADCC treatment (Figure S6A–D). Hence, a single intraperitoneal injection of anti-VSIG4-ADCC allows the generation of a peritoneal cavity that lacks VSIG4⁺ LPMs, without affecting the total percentage of LPMs or KCs.

Using this strategy, VSIG4⁺ LPMs were depleted seven days prior to the *T. b. brucei* infection. At d5 and d6 post-infection, an increased peak parasitemia was observed in mice that received the VSIG4-depleting construct (Figure 4D), suggesting the contribution of VSIG4⁺ LPMs to early parasite elimination. However, no increased parasitemia was observed at later stages and the mice survived equally long (Figure 4E). The lack of long-term effects of experimental VSIG4⁺ LPM depletion on infection parameters is in line with the fact that *T. b. brucei* naturally downscales the presence of these cells. Indeed, in female C57BL/6 hosts, the VSIG4⁺ LPM population nearly disappeared at d8, to return to approximately 25% of the total LPM population by d29 (Figure 4F), albeit with a strongly reduced VSIG4 surface expression level (Figure 4G). Hence, VSIG4⁺ LPMs contribute to parasite elimination in the early phase of infection.

2.4 | VSIG4+ LPMs are Superior in Phagocytosing CRC Cancer Cells and Protect Against CRC Peritoneal Tumor Outgrowth

Since the PC is a common metastatic site for CRC [25, 26], it can be questioned whether VSIG4⁺ LPMs play a role in the establishment and growth of CRC peritoneal metastases.

Human peritoneal macrophages were shown before to express VSIG4 in healthy conditions [27]. We now assessed whether the VSIG4 receptor is expressed on macrophages associated with peritoneal metastatic nodules of CRC cancer patients, in comparison to their primary tumor. Macrophages were identified as CD45⁺ CD11b⁺ CD66b⁻ CD14⁺ HLA-DR⁺ CD163⁺ cells (Figure S7) and their percentage (within CD45⁺) was on average higher in CRC metastatic nodules in the omentum (O) and mesentery (M) as compared with the primary tumor (PT) (Figure 5A). Importantly, VSIG4⁺ macrophages were present in both the metastatic nodules and the primary tumor (Figure 5B), suggesting a potential involvement of these cells in the metastatic process.

To investigate the role of VSIG4⁺ LPMs in a mouse model of CRC peritoneal metastasis, mouse MC38-Thy1.1⁺ CRC cancer

**FIGURE 3** | VSIG4$^+$ LPMs influence the early phase of *Trypanosoma brucei brucei* infections. (A) Absolute cell number of LPMs, (B) VSIG4$^+$ LPMs and (C) VSIG4 expression level in VSIG4$^+$ LPMs depicted as ΔMFI in peritoneal lavages of female C57BL/6 mice 18 h post i.p. injection of *Trypanosoma brucei brucei* or HBSS (naive) ($n = 3$/group). (D) UMAP plot of LPM clusters obtained via CITE-sequencing of peritoneal exudate cells from HBSS-injected ($n = 3$) and *T. brucei brucei*-infected mice ($n = 3$). (E) Dot plot of highly expressed markers per LPM subset, following CITE-sequencing of HBSS-injected ($n = 3$) and *T. brucei brucei*-infected mice ($n = 3$). The size of the dot indicates the expression percentage in the LPM subset, while the color indicates the average expression level. (F) Feature plot of *Vsig4* mRNA and VSIG4 protein expression in LPM subsets of *T. brucei brucei*-infected mice. Volcano plot of DEGs (G) and DEPs (H) between VSIG4$^+$ LPMs of HBSS-injected and *T. brucei brucei*-infected mice, and (I) DEGs and (J) DEPs between VSIG4$^+$ and VSIG4$^-$ LPMs of *T. brucei brucei*-infected mice, whereby the adjusted *p*-value is plotted versus the fold change. LPMs were divided into VSIG4$^+$ and VSIG4$^-$ LPMs based on the protein expression cut-off of >3.5 and <3.0, respectively. Unpaired two-tailed Student's *t*-tests were performed. The *p*-value is shown on the graphs as such: *$p \leq 0.05$, **$p \leq 0.01$, ***$p \leq 0.001$, ****$p \leq 0.0001$. Data are shown as the mean ± SEM.

cells were injected into the PC. In this model, MC38-Thy1.1$^+$ nodules were present in the omentum as early as 6 days postinjection, which further increased by day 16 (Figure 5C). These nodules contained ICAM2$^+$ metastasis-associated macrophages (MAMs), a percentage of which also expressed the VSIG4 receptor (Figure 5D,E). In the first setting, VSIG4$^+$ LPMs were depleted by injecting the anti-VSIG4-ADCC construct 7 days prior to MC38-Thy1.1$^+$ cancer cell injection (Figure 6A), at which point the cancer cells were confronted with a PC largely devoid of VSIG4$^+$ LPMs while the total LPM pool and the KC pool was unaltered (Figure 4B,C, Figure S6). As a control, the anti-VSIG4-LALAPG ADCC-disabled construct was injected. Prior depletion of VSIG4$^+$ LPMs resulted in a significantly decreased survival compared with control mice, suggesting that VSIG4$^+$ LPMs play a protective role during MC38 growth in the PC (Figure 6B). To assess the effect of VSIG4$^+$ LPM depletion when tumors were initiated, we treated mice with anti-VSIG4-ADCC or the non-depleting control construct 2 days after the intraperitoneal cancer cell inoculation (Figure 6C). Again, the depletion of VSIG4$^+$ LPMs resulted in decreased survival compared with control mice (Figure 6D). Together, these data demonstrate the protective role of VSIG4$^+$ LPMs against CRC tumor outgrowth in the PC.

To mechanistically underpin these findings, we assessed the phagocytic capacity of VSIG4$^+$ and VSIG4$^-$ LPMs toward MC38-Thy1.1$^+$ cancer cells. Hereto, DiO-labeled MC38-Thy1.1$^+$ cancer cells were co-cultured for 1 h with peritoneal exudate cells, after which the DiO-positivity of VSIG4$^+$ and VSIG4$^-$ LPMs was assessed via flow cytometry. Interestingly, VSIG4$^+$ LPMs displayed a significantly enhanced capacity to phagocytose MC38-Thy1.1$^+$ cancer cells compared with VSIG4$^-$ LPMs (Figure 6E,F), possibly explaining their importance as antitumoral cells in the PC. Of note, the phagocytic capacity of VSIG4$^+$ LPMs toward MC38-Thy1.1$^+$ cancer cells was not significantly affected by age, suggesting that the VSIG4$^+$ LPM population expands in function over time without altering their intrinsic functionality (Figure S2E).

3 | Discussion

To date, the function of the VSIG4 receptor has been mostly described in the liver, where it is expressed by the entire liver-resident KC population and is involved in complement-dependent and -independent pathogen recognition. We and
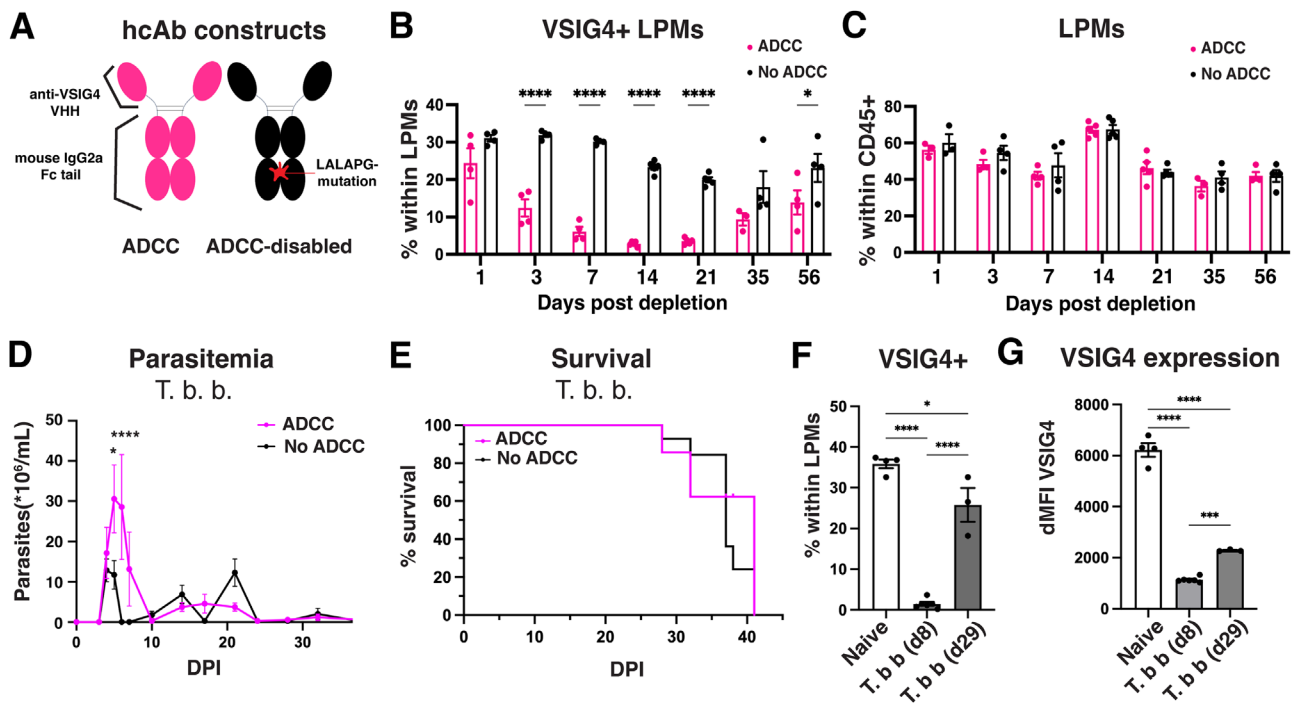
FIGURE 4 | Depletion of VSIG4$^+$ LPMs during a *Trypanosoma brucei brucei* infection increases the first peak of parasitemia. (A) Schematic representation of the ADCC-enabled (pink) and ADCC-disabled (black) anti-VSIG4 constructs. (B) Percentage of VSIG4$^+$ LPMs within all LPMs and (C) percentage of LPMs within CD45$^+$ peritoneal exudate cells of naive C57BL/6 mice at different intervals following a single i.p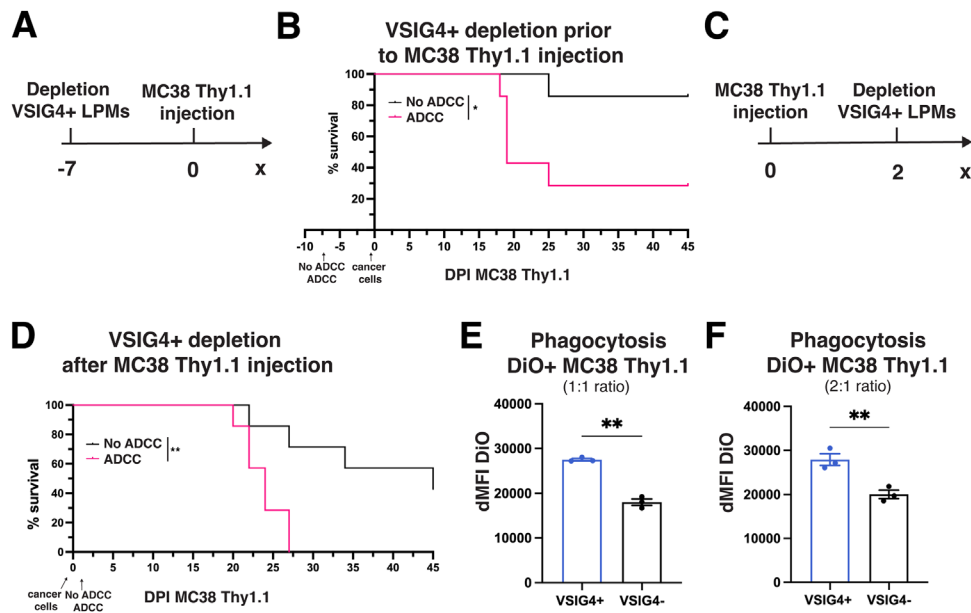. injection of the anti-VSIG4 ADCC-enabled (pink) or ADCC-disabled (black) construct ($n = 4$/group). Data are representative of two independent experiments. (D) Parasitemia in the blood and (E) Kaplan–Meier survival curve of C57BL/6 mice that received a single i.p. injection of the anti-VSIG4 ADCC-enabled (pink) or ADCC-disabled (black) construct 7 days prior to the *T. brucei brucei*-infection ($n = 7$/group). (F) Percentage of VSIG4$^+$ LPMs within all LPMs and (G) VSIG4 expression level in VSIG4$^+$ LPMs depicted as ΔMFI, in naive ($n = 4$), 8 days post-*T. brucei brucei* infection ($n = 6$) and 29 days postinfection ($n = 3$) C57BL/6 mice. A one-way ANOVA was performed with the Tukey multiple comparisons test (F, G), or a two-way ANOVA with the Sidak multiple comparisons test was performed (B–D). Survival curves were analyzed using the log-rank (Mantel–Cox) test (E). The *p*-value is shown on the graphs as such: *$p \leq 0.05$, **$p \leq 0.01$, ***$p \leq 0.001$, ****$p \leq 0.0001$. Data are shown as the mean ± SEM.
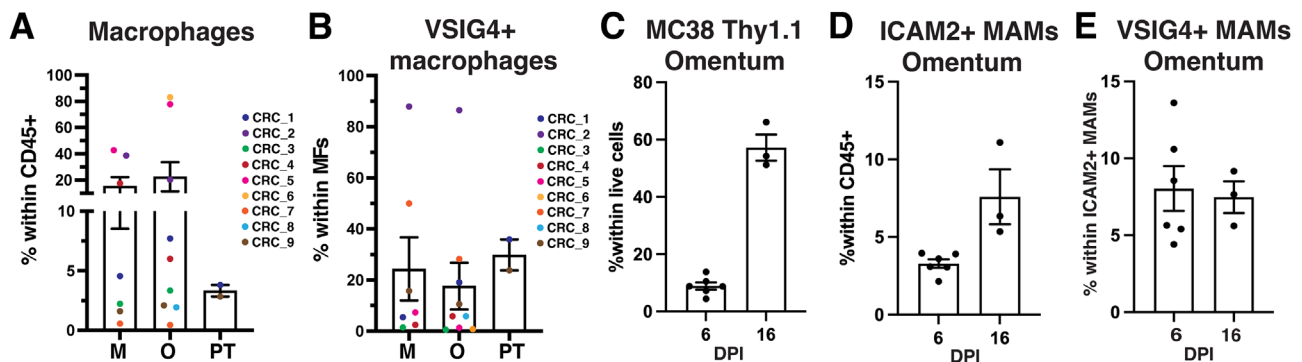
FIGURE 5 | VSIG4$^+$ macrophages are present in peritoneal metastasis of CRC patients and a murine model of CRC metastasis. (A) Percentage of macrophages within CD45$^+$ cells and (B) VSIG4$^+$ macrophages within all macrophages in the primary tumor (PT) and metastasis to the mesentery (M) and omentum (O) of 9 patients with metastasized colorectal cancer. Each datapoint corresponds to an independent patient sample. (C) Percentage of MC38-Thy1.1 cells within all live cells in the omentum, (D) percentage of ICAM2$^+$ metastasis-associated macrophages (MAMs) within CD45$^+$ cells and (E) percentage of VSIG4$^+$ MAMs within all MAMs following 6 days ($n = 6$) and 16 days ($n = 3$) post-MC38-Thy1.1 injection (days postinjection, DPI) in C57BL/6 mice. Data are representative of two independent experiments. Data are shown as the mean ± SEM.

others showed that approximately 30% of the LPMs in the PC also express the VSIG4 receptor, but its regulation and function on those cells and the significance of VSIG4$^+$ LPMs during steady-state or peritoneal infectious or cancerous disease is unknown.

A remarkable finding is that the majority of VSIG4$^+$ LPMs were of embryonic origin, while most of the VSIG4$^-$ LPMs were of monocytic origin. This could possibly be explained by a steady turnover of embryonically derived LPMs by monocyte-derived LPMs, whereby VSIG4 expression is only slowly gained by the

FIGURE 6 | VSIG4+ LPMs are superior in phagocytosing CRC cancer cells and protect against CRC peritoneal metastasis. (A) Schematic representation of the cancer cell and anti-VSIG4 construct injection regimen of the experiment shown in panel B. (B) Kaplan–Meier survival curve of C57BL/6 mice that received an i.p. injection of the anti-VSIG4 ADCC-enabled (pink) or ADCC-disabled (black) construct 7 days prior to MC38-Thy1.1 cancer cell injection ($n = 7$/group). Data are representative of two independent experiments. (C) Schematic representation of the cancer cell and anti-VSIG4 construct injection regimen of the experiment shown in panel D. (D) Kaplan–Meier survival curve of C57BL/6 mice that received an intraperitoneal injection of the anti-VSIG4 ADCC-enabled (pink) or ADCC-disabled (black) construct 2 days after MC38-Thy1.1 cancer cell injection ($n = 7$/group). Data are representative of two independent experiments. In vitro phagocytosis of DiO-labeled MC38-Thy1.1 cancer cells, (E) at a ratio of 1:1 (peritoneal exudate cells:cancer cells), or **(F)** at a ratio of 2:1 (peritoneal exudate cells: cancer cells), depicted as ΔMFI of the DiO signal in VSIG4+ and VSIG4− LPMs. Unlabeled MC38-Thy1.1 cancer cells were used as a negative control for the DiO signal ($n = 3$/group). Survival curves were analyzed using the log-rank (Mantel-Cox) test (B, D). Unpaired two-tailed Student's t-tests were performed (E, F). The p-value is shown on the graphs as such: *$p \leq 0.05$, **$p \leq 0.01$, ***$p \leq 0.001$, ****$p \leq 0.0001$. Data are shown as the mean ± SEM.

monocyte-derived cells. In accordance, Louwe et al. demonstrated that the time of residency in the PC is a determining factor for the expression of LPM markers such as VSIG4, Tim4, and CD209b[28]. When VSIG4+ LPMs were depleted, VSIG4 expression was not regained for at least 3 weeks, and even at d56, the level of VSIG4+ LPMs did not yet reach steady-state levels, again suggesting a slow acquisition of the VSIG4 receptor. Finally, also the fact that VSIG4+ LPMs are somewhat less abundant in the PC of male mice could be in line with a slow VSIG4 acquisition since LPMs in male mice have a higher turnover rate than in female mice [14]. Another factor that could influence VSIG4 expression is the presence of microbiota, whose metabolic products were shown before to affect the functionality of tissue-resident macrophages [18]. Interestingly, although the formation of VSIG4+ LPMs is not affected in germ-free conditions, their VSIG4 expression level is higher, suggesting that a tonic exposure to microbiota-derived molecules, either metabolic or structural, downregulates VSIG4 expression or increases its internalization.

However, if such a tonic triggering of VSIG4 in LPMs exists, it would not lead to intracellular signaling and an altered gene expression. Indeed, we were unable to find any DEGs or DEPs to discern VSIG4+ from VSIG4− LPMs at steady-state, suggesting that the VSIG4 receptor does not delineate a unique LPM subset. Nevertheless, VSIG4+ LPMs were superior phagocytic cells, implying that these cells could play a protective role during infectious and neoplastic disease in the PC. The specific depletion

of VSIG4+ LPMs via our in-house generated anti-VSIG4-ADCC construct resulted in a higher first peak of parasitemia upon intraperitoneal *T. b. brucei* infection, as well as a decreased survival upon MC38 CRC inoculation in the PC. The survival of *T. b. brucei*-infected mice was not affected by the absence of VSIG4+ LPMs despite the observed increased parasitemia in mice that lack VSIG4+ LPMs. Although the cause of death of mice infected with trypanosomes is not fully understood, we hypothesize that multiorgan failure [29, 30] and neuroinflammation [31] mainly contribute to their mortality, which is uncoupled from parasite load in the blood.

The protective effect of VSIG4+ LPMs against peritoneal CRC tumor outgrowth is in line with findings demonstrating the LPM-mediated phagocytosis of metastasizing cancer cells in a model of ovarian cancer (ID8), whereby LPMs also play an important role in the early phases of cancer cell dissemination [11]. In patients with chronic liver disease that develop ascites, VSIG4+ macrophages were also found to be highly phagocytic compared with VSIG4− monocyte-derived macrophages [32]. In contrast, other studies claimed that LPMs support cancer cell metastasis and negatively affect antitumor T-cell immunity in cancer patients with peritoneal metastases [33, 34]. Of note, VSIG4+ macrophages are also found in primary CRC tumors, where this marker mostly associates with C1Q, CD206, and CD163-expressing macrophages that display a tumor-promoting phenotype and whose presence has been associated with a worse

outcome in several cancer types, including CRC and peritoneal metastasis [35–37]. It will be interesting to assess whether our anti-VSIG4-ADCC construct or another approach that specifically depletes VSIG4$^+$ cells, will be of therapeutic use against primary CRC tumors. However, such an approach holds the risk of increasing death due to peritoneal metastasis, as shown in this manuscript.

Altogether, our work sheds new light on the characteristics of VSIG4$^+$ LPMs, identifying these cells as contributors to antiparasitic and antimetastatic responses in the peritoneal cavity.

3.1 | Study Limitations

While this study sheds light on the role of VSIG4-expressing LPMs in steady state and inflammation, limitations must be considered. The expression of the VSIG4 receptor on LPMs is likely environment-driven, as monocyte-derived macrophages can acquire VSIG4 in function of time. The environmental factors that drive the abundance of VSIG4$^+$ LPMs and the VSIG4 expression level have not been identified in this study, as ontogeny, gender, and microbiota do not drastically affect the abundance of VSIG4$^+$ LPMs and their VSIG4 expression level. To determine the ontogeny of VSIG4$^+$ LPMs, Flt3-Cre x Rosa26-YFP reporter mice were used which limited our study to the use of male mice since the Flt3-Cre transgene is located on the Y-chromosome.

In a steady state and after the introduction of an inflammatory stimulus, VSIG4-expressing LPMs and their negative counterparts are similar at the transcriptomic and proteomic levels, at least within the time window that we collected the LPMs. It cannot be excluded that differences between VSIG4$^+$ and VSIG4$^-$ LPMs could be discovered at different timepoints of LPM collection or in different models of inflammation than the ones used in this study.

Finally, while we demonstrated that VSIG4$^+$ LPMs play a protective role in a murine model of CRC metastasis, no functional evidence is provided yet that would suggest an equally protective role for VSIG4$^+$ MAMs in cancer patients, beyond the mere presence of such VSIG4$^+$ MAMs in metastatic lesions of CRC cancer patients.

4 | Materials and Methods

4.1 | Mice

VSIG4$^{-/-}$[3], VISG4$^{+/+}$, Flt3Cre [38], and Rosa26-YFP [39] mice were bred in-house. C57BL/6 mice were purchased from Janvier, France.

4.2 | Cell Culture and Tumor Models

The MC38 cell line was kindly provided by Massimiliano Mazzone (VIB-KULeuven, Belgium). The MC38 cell line was plated and cultured in DMEM supplemented with 10% FCS, Pen/Strep, and glutamine at 37°C and 5% CO_2. 10^6 MC38-Thy1.1 cells were

injected intraperitoneally in 200 μL HBSS to mimic peritoneal metastasis of colorectal cancer cells.

4.3 | Trypanosoma Infection

Bloodstream trypanosome parasites were stored at $-80\,°C$ as blood aliquots containing 50% Alsever's solution (Sigma–Aldrich) and 10% glycerol (final v/v). Clonal pleomorphic *T. brucei* AnTat1.1E parasites were gifted by N. Van Meirvenne (Institute for Tropical Medicine, Belgium), and clonal *T. congolense* parasites (Tc13) were gifted by Dr. Henry Tabel (University of Saskatchewan, Canada). 6- to 12-week-old female mice were infected with 5000 trypanosomes via intraperitoneal injection of 200 μL PBS. Parasite numbers in the blood were counted using a hemocytometer.

4.4 | Ex Vivo Preparation of Single Cell Suspensions, Flow Cytometry, and Sorting

Processing of organs and subsequent flow cytometry analysis or sorting of cells is described in the supplementary data, including a list of antibodies used (Table S1).

4.5 | Phagocytosis Assay

pHrodo Red *E. coli* Bioparticles (Thermofisher, P35361) and pHrodo Red *S. aureus* Bioparticles (Thermofisher, A10010) were prepared according to the manufacturer's manual and injected intraperitoneally at 500 μg/mL in 500 μL HBSS. As a negative control, HBSS or unlabeled bioparticles were injected (Thermofischer, S2859).

DiO cell labeling (Thermofischer, V22886) was prepared according to the manufacturer's manual. MC38-Thy1.1 cancer cells were incubated with DiO dye (2.5 μM) for 20 min at 37°C. The cancer cells were washed and spun down for 6 min at room temperature and 450G. The cancer cells were cocultured in sterile capped polystyrene tubes with peritoneal exudate cells in DMEM medium (Gibco) and a 37°C-incubator for 1 h at 5% CO_2. After incubation, the cells were washed with FACS buffer (1% FCS, 2 mM EDTA) and prepared for antibody staining and flow cytometry analysis, as described in the supplementary materials and methods.

4.6 | Sample Processing for CITE-Sequencing

Peritoneal lavages were collected in 10 mL ice-cold HBSS supplemented with 30 μM actinomycin D. Three peritoneal lavages were pooled for each condition (HBSS-injected naive versus 18 h post-*T. brucei brucei* infection). The single cell suspensions were stained with APC-Cy7-labeled anti-CD45 (30-F11), viability dye 7-Actinomycin D, TruStain FcX PLUS (Biolegend) and oligo-conjugated CITE-seq antibodies (Table S2) in FACS buffer (HBSS, 1% FCS and 2 mM EDTA) supplemented with 3 μM actinomycin D. After washing with FACS buffer, approximately 50,000 live CD45+ cells were sorted into FACS buffer (3 μM actinomycin D) using the BD FACSAria III (BD Biosciences). The sorted cells

were subsequently spun down and resuspended in PBS (0.04% BSA, 3 μM actinomycin D) at an estimated final concentration of 1000 cells/μL. GEMs and CITE-seq libraries were prepared using a Chromium Next GEM Single Cell 3' Gel Bead and Library kit, v3.1 as previously described [17]. The processing of CITE-sequencing data is described in the Supporting Information Materials.

4.7 | Retrieval of Published scRNAseq Datasets

RNA expression matrices of a scRNA-seq dataset of naive $CD102^+$ peritoneal macrophages of male and female mice were obtained from the Gene Expression Omnibus (GEO) database (GSE149014) [14]. The processing of scRNA-seq datasets is described in the supplementary materials.

4.8 | Anti-VSIG4 Constructs

The anti-VSIG4 Nanobody (Nb119) was obtained as previously described [23]. The anti-VSIG4 Nb sequence was cloned into a vector followed by a GlySer linker (10GS) and the WT or LALAPG-mutated Fc region of mouse IgG2a, resulting in the anti-VSIG4-ADCC and anti-VSIG4 ADCC-disabled constructs. The methods for generating, expressing, and purifying the anti-VSIG4 constructs are provided in the Supporting Information Materials. $VSIG4^+$ LPMs were depleted via intraperitoneal injection of 200 μg of anti-VSIG4-ADCC in 200 μL HBSS. Injection regimens are shown in Figure 6A,C.

4.9 | Ex Vivo Analysis of Human CRC Tissue

Fresh tumor tissue was obtained from 9 cancer patients with colorectal cancer metastasis to the omentum and mesentery. Surgical resection occurred at Ghent University Hospital (GI Surgery). Samples were transported on ice to the research facility at the Vrije Universiteit Brussel and processed for flow cytometry analysis. Single-cell suspensions were prepared as previously described [40].

4.10 | Statistics

Data is demonstrated as the mean ± standard error of the mean (SEM). GraphPad Prism 9.5.1 was used to calculate statistical significance. For pairwise comparisons, an unpaired two-tailed Student's t-test was performed. For the comparison of one or multiple groups, either a one-way analysis of variance (ANOVA) was performed with the Tukey multiple comparisons test or a two-way ANOVA with the Sidak multiple comparisons test was performed. Survival curves were analyzed using the log-rank (Mantel–Cox) test. In case of statistically significant differences, the p-value is shown on the graphs as such: $*p \leq 0.05$, $**p \leq 0.01$, $***p \leq 0.001$, $****p \leq 0.0001$. Outliers were identified using the Iterative Grubbs' method with alpha at 0.2.

Author Contributions

Els Lebegge: Conceptualization, performed experiments, analyzed and visualized data, and wrote the manuscript. Sana M. Arnouk: Performed experiments and revised the manuscript. Maté Kiss, Jolien Van Craenenbroeck, Romina Mora Barthelmess, Neema Ahishakiye Jumapili, Maida Zivalj, Naela Assaf, Yvon Elkrim, Eva Hadadi, Leen Ali: Performed experiments. Daliya Kancheva: Analyzed scRNAseq data. Kiavash Mohavedi, Benoit Stijlemans, Eva Hadadi, Cécile Vincke, Geert Raes, and Damya Laoui: Conceptualization. Jo A. Van Ginderachter: Conceptualization, obtained funding support, supervised the study, and wrote and revised the manuscript.

Conflicts of Interest

The authors declare no conflicts of interest.

Data Availability Statement

Supplementary Information is available on the European Journal of Immunology website. The data that support the findings of this study are available upon request from the corresponding author. CITE-seq data are deposited in a public repository (GSE295757).

Ethics Statement

Animal experiments were approved by the Ethical Commission for Animal Welfare at the Vrije Universiteit Brussel and performed in accordance with the guidelines set by the Belgian Council for Laboratory Animal Science. Human samples were obtained in accordance with the ethical guidance provided by the Declaration of Helsinki. Patients undergoing surgery for peritoneal metastasis provided written informed consent. The experimental protocol and informed consent documents were approved by the institutional review board (IRB) of Ghent University Hospital (ref. BC-06978).

References

1. E. E. B. Ghosn, A. A. Cassado, G. R. Govoni, et al., "Two Physically, Functionally, and Developmentally Distinct Peritoneal Macrophage Subsets," *Proceedings of the National Academy of Sciences* 2010, 107 (6), 2568–2573, https://doi.org/10.1073/pnas.0915000107.

2. L. Salm, R. Shim, N. Noskovicova, and P. Kubes, "Gata6+ Large Peritoneal Macrophages: An Evolutionarily Conserved Sentinel and Effector System for Infection and Injury," *Trends in Immunology* 44, no. 2 (2023): 129–145.

3. K. Y. Helmy, K. J. Katschke, N. N. Gorgani, et al., "CRIg: A Macrophage Complement Receptor Required for Phagocytosis of Circulating Pathogens," *Cell* 124, no. 5 (2006): 915–927.

4. L. Vogt, N. Schmitz, M. O. Kurrer, et al., "VSIG4, a B7 Family-Related Protein, Is a Negative Regulator of T Cell Activation," *Journal of Clinical Investigation* 116, no. 10 (2006): 2817–2826.

5. Z. Zeng, B. G. J. Surewaard, C. H. Y. Wong, J. A. Geoghegan, C. N. Jenne, and P. Kubes, "CRIg Functions as a Macrophage Pattern Recognition Receptor to Directly Bind and Capture Blood-Borne Gram-Positive Bacteria," *Cell Host & Microbe* 20, no. 1 (2016): 99–106.

6. J. Li, B. Diao, S. Guo, et al., "VSIG4 Inhibits Proinflammatory Macrophage Activation by Reprogramming Mitochondrial Pyruvate Metabolism," *Nature Communications* 8, no. 1 (2017): 1322.

7. A. Widyagarini, N. Nishii, Y. Kawano, C. Zhang, and M. Azuma, "VSIG4/CRIg Directly Regulates Early CD8+ T Cell Activation Through Its Counter-Receptor in a Narrow Window," *Biochemical and Biophysical Research Communications* 614 (2022): 100–106.

8. X. Zang and J. P. Allison, "To Be or Not to Be B7," *Journal of Clinical Investigation* 116, no. 10 (2006): 2590–2593.

9. B. Liu, L. Cheng, H. Gao, et al., "The Biology of VSIG4: Implications for the Treatment of Immune-Mediated Inflammatory Diseases and Cancer," *Cancer Letters* 553 (2023): 215996.

10. K. Wong, P. A. Valdez, C. Tan, S. Yeh, J.-A. Hongo, and W. Ouyang, "Phosphatidylserine Receptor Tim-4 Is Essential for the Maintenance of the Homeostatic State of Resident Peritoneal Macrophages," *The Proceedings of the National Academy of Sciences* 2010, 107 (19), 8712–8717, https://doi.org/10.1073/pnas.0910929107.

11. S. Joshi, L. López, L. G. Morosi, et al., "Tim4 Enables Large Peritoneal Macrophages to Cross-Present Tumor Antigens at Early Stages of Tumorigenesis," *Cell reports* 43, no. 4 (2024): 114096.

12. T. Ito, Y. Shintani, L. Fields, et al., "Cell Barrier Function of Resident Peritoneal Macrophages in Post-Operative Adhesions," *Nature Communications* 12, no. 1 (2021): 2232.

13. S. Stengel, S. Quickert, P. Lutz, et al., "Peritoneal Level of CD206 Associates with Mortality and an Inflammatory Macrophage Phenotype in Patients with Decompensated Cirrhosis and Spontaneous Bacterial Peritonitis," *Gastroenterology* 158, no. 6 (2020): 1745–1761.

14. C. C. Bain, D. A. Gibson, N. J. Steers, et al., "Rate of Replenishment and Microenvironment Contribute to the Sexually Dimorphic Phenotype and Function of Peritoneal Macrophages," *Science Immunology* 5, no. 48 (2020): eabc4466.

15. C. C. Bain, C. A. Hawley, H. Garner, et al., "Long-Lived Self-Renewing Bone Marrow-Derived Macrophages Displace Embryo-Derived Cells to Inhabit Adult Serous Cavities," *Nature Communications* 7, no. 1 (2016): ncomms11852.

16. Y. Okabe and R. Medzhitov, "Tissue-Specific Signals Control Reversible Program of Localization and Functional Polarization of Macrophages," *Cell* 157, no. 4 (2014): 832–844.

17. M. A. Musrati, B. Stijlemans, A. Azouz, et al., "Infection History Imprints Prolonged Changes to the Epigenome, Transcriptome and Function of Kupffer Cells," *Journal of Hepatology* (2024): S0168827824023638.

18. P. H. V. Saavedra, A. Trzeciak, Z. Wang, et al.,A Microbiota-Derived Metabolite Instructs Peripheral Efferocytosis, August 18, 2022, https://doi.org/10.1101/2022.08.17.504322.

19. M. Guilliams, J. Bonnardel, B. Haest, et al., "Spatial Proteogenomics Reveals Distinct and Evolutionarily Conserved Hepatic Macrophage Niches," *Cell* 185, no. 2 (2022): 379–396.e38.

20. A. L. Coelho, M. A. Schaller, C. F. Benjamim, A. Z. Orlofsky, C. M. Hogaboam, and S. L. Kunkel, "The Chemokine CCL6 Promotes Innate Immunity via Immune Cell Activation and Recruitment," *Journal of Immunology* 179, no. 8 (2007): 5474–5482.

21. Y. Peng, Y. Fang, Z. Li, C. Liu, and W. Zhang, "Saa3 Promotes Pro-Inflammatory Macrophage Differentiation and Contributes to Sepsis-Induced AKI," *International Immunopharmacology* 127 (2024): 111417.

22. N. Itami, Y. Kondo, S. Tademoto, D. Ito, S. Fukumoto, and H. Otsuki, "Alternative Activation of Macrophages in Mice Peritoneal Cavities and Diaphragms by Newborn Larvae of *Trichinella Spiralis*," *Yonago Acta Medica* 63, no. 1 (2020): 34–41.

23. F. Zheng, S. Put, L. Bouwens, et al., "Molecular Imaging With Macrophage CRIg-Targeting Nanobodies for Early and Preclinical Diagnosis in a Mouse Model of Rheumatoid Arthritis," *Journal of Nuclear Medicine* 55, no. 5 (2014): 824–829.

24. I. Wilkinson, S. Anderson, J. Fry, et al., "Fc-Engineered Antibodies With Immune Effector Functions Completely Abolished," *PLoS ONE* 16, no. 12 (2021): e0260954.

25. W. Ceelen, R. G. Ramsay, V. Narasimhan, A. G. Heriot, and O. De Wever, "Targeting the Tumor Microenvironment in Colorectal Peritoneal Metastases," *Trends in cancer* 6, no. 3 (2020): 236–246.

26. K. J. Lenos, S. Bach, L. Ferreira Moreno, et al., "Molecular Characterization of Colorectal Cancer Related Peritoneal Metastatic Disease," *Nature Communications* 13, no. 1 (2022): 4443.

27. J. Reißing, P. Lutz, M. Frissen, et al., "Immunomodulatory Receptor VSIG4 Is Released During Spontaneous Bacterial Peritonitis and Predicts Short-Term Mortality," *JHEP Rep Innov Hepatol* 4, no. 1 (2022): 100391.

28. P. A. Louwe, L. Badiola Gomez, H. Webster, et al., "Recruited Macrophages That Colonize the Post-Inflammatory Peritoneal Niche Convert Into Functionally Divergent Resident Cells," *Nature Communications* 12, no. 1 (2021): 1770.

29. S. Magez, B. Stijlemans, G. Caljon, H.-P. Eugster, and P. De Baetselier, "Control of Experimental Trypanosoma Brucei Infections Occurs Independently of Lymphotoxin-α Induction," *Infection and Immunity* 70, no. 3 (2002): 1342–1351.

30. B. Stijlemans, P. De Baetselier, S. Magez, J. A. Van Ginderachter, and C. De Trez, "African Trypanosomiasis-Associated Anemia: The Contribution of the Interplay Between Parasites and the Mononuclear Phagocyte System," *Frontiers in immunology* 9 (2018): 218.

31. K. De Vlaminck, H. Van Hove, D. Kancheva, et al., "Differential Plasticity and Fate of Brain-Resident and Recruited Macrophages During the Onset and Resolution of Neuroinflammation," *Immunity* 55, no. 11 (2022): 2085–2102.e9.

32. K. M. Irvine, X. Banh, V. L. Gadd, et al., "CRIg-Expressing Peritoneal Macrophages Are Associated With Disease Severity in Patients With Cirrhosis and Ascites," *JCI Insight* 1, no. 8 (2016).

33. A. Chow, S. Schad, and M. D. Green, et al., "Tim-4+ Cavity-Resident Macrophages Impair Anti-Tumor CD8+ T Cell Immunity," *Cancer Cell* 2021, 39 (7), 973–988.e9, https://doi.org/10.1016/j.ccell.2021.05.006.

34. H. Xia, S. Li, X. Li, et al., "Autophagic Adaptation to Oxidative Stress Alters Peritoneal Residential Macrophage Survival and Ovarian Cancer Metastasis," *JCI Insight* 5, no. 18 (2020): e141115.

35. L. Zhang, Z. Li, K. M. Skrzypczynska, et al., "Single-Cell Analyses Inform Mechanisms of Myeloid-Targeted Therapies in Colon Cancer," *Cell* 181, no. 2 (2020): 442–459.e29.

36. L. T. Roumenina, M. V. Daugan, R. Noé, et al., "Tumor Cells Hijack Macrophage-Produced Complement C1q to Promote Tumor Growth," *Cancer immunology research* 7, no. 7 (2019): 1091–1105.

37. Y. Li, L. Jiang, Y. Chen, et al., "Specific Lineage Transition of Tumor-Associated Macrophages Elicits Immune Evasion of Ascitic Tumor Cells in Gastric Cancer With Peritoneal Metastasis," *Gastric Cancer* 2024, 27 (3), 519–538, https://doi.org/10.1007/s10120-024-01486-6.

38. C. Benz, V. C. Martins, F. Radtke, and C. C. Bleul, "The Stream of Precursors That Colonizes the Thymus Proceeds Selectively Through the Early T Lineage Precursor Stage of T Cell Development," *Journal of Experimental Medicine* 205, no. 5 (2008): 1187–1199.

39. S. Srinivas, T. Watanabe, C.-S. Lin, et al., "Cre Reporter Strains Produced by Targeted Insertion of EYFP and ECFP Into the ROSA26 Locus," *BMC Developmental Biology* 1, no. 1 (2001): 4.

40. D. Laoui, J. Keirsse, Y. Morias, et al., "The Tumour Microenvironment Harbours Ontogenically Distinct Dendritic Cell Populations With Opposing Effects on Tumour Immunity," *Nature Communications* 7, no. 1 (2016): 13720.

Supporting Information

Additional supporting information can be found online in the Supporting Information section.